

Macroscopic equations for pattern formation in mixtures of microtubules and motors

Ha Youn Lee¹ and Mehran Kardar^{1,2}

¹*Department of Physics, Massachusetts Institute of Technology, Cambridge, Massachusetts 02139*

²*Institute for Theoretical Physics, University of California, Santa Barbara, California 93106*

Inspired by patterns observed in mixtures of microtubules and molecular motors, we propose continuum equations for the evolution of motor density, and microtubule orientation. The chief ingredients are the transport of motors along tubules, and the alignment of tubules in the process. The macroscopic equations lead to aster and vortex patterns in qualitative agreement with experiments. While the early stages of evolution of tubules are similar to coarsening of spins following a quench, the rearrangement of motors leads to arrested coarsening at low densities. Even in one dimension, the equations exhibit a variety of interesting behaviors, such as symmetry breaking, moving fronts, and motor localization.

PACS numbers: 87.10+e, 87.15-v, 05.10-a

I. INTRODUCTION

The emergence of complex patterns and correlated fluctuations is a characteristic of many out of equilibrium situations [1,2]. Living organisms provide many examples, ranging from the flocking of birds [3,4], the social organization of bacterial colonies [5–7], to internal reorganization of a cell during division [8,9].

At the molecular level, motors and microtubules are frequently the ingredients responsible for construction and motion. Molecular motors are the proteins that convert chemical energy to mechanical energy, and have been extensively studied [10–12]. Microtubules, consisting of a subunit protein called tubulin provide the scaffolding for many cell constructs, as well as “railways” for transport of proteins [13,14]. In particular, microtubules have a polarity that provides a direction for the transport of motors.

One of the many processes in which motors and microtubules are involved is cell division. They are indeed the main ingredients of mitotic spindles which serve to move apart the duplicated chromosomes of eucaryotic cells [8,9]. To elucidate some of the physical mechanisms involved, several *in vitro* experiments on mixtures of microtubules and motors have been carried out [15–17]. Even these simple mixtures result in interesting patterns: At an initial stage the microtubules form an aster with their “plus” ends pointing towards a center. The kinesin based beads move along the microtubules towards this center. In a confined geometry, the aster pattern is then destabilized, giving way to a vortex in which the motors rotate around a center. At larger scales and in unconfined geometries, a variety of self-organized patterns are obtained upon varying the motor concentration. With increasing concentration, an array of vortices, a mixture of asters and vortices, a collection of asters, and bundles of microtubules emerge.

The motivation of this paper is to describe some of

the patterns observed in these experiments. There are in fact already several models of these phenomena in the literature, starting with the simulations reported in the original paper on the patterns [16]. A two-dimensional model for the orientations of microtubules was used to produce inhomogeneous stripe patterns [18]. Another recent model introduces a convection-diffusion equation for motor density in the presence of the microtubule array. This model results in a density profile of motors in asters which decays as a power-law [19].

Our approach is to take a macroscopic perspective, introducing two continuous fields $m(\vec{r}, t)$ and $\vec{T}(\vec{r}, t)$ to describe the local motor density and tubule orientation, respectively. The central input to these equations is that the motor density is transported along the tubule direction, while the tubules are in turn aligned by the motors. In the *in vitro* experiments [16], the physical origin of the latter is that the motor complexes can attach to two nearby tubules and their motion along the two provides a force that makes them parallel [20]. In writing such continuum equations for densities, we are following recent studies modeling the flocking of birds [3,4], and the organization of growing bacteria [5–7]. Simulations of these equations reproduce asters and vortices in agreement with experiment. Analytical solutions also provide further insights on the patterns. For example, we find that the motor density is much larger close to the center of an aster, than in a vortex. The resulting increased strain energy on the tubules provides a driving force for asters to break off to form vortices, in qualitative agreement with experiments.

The global evolution of the tubule pattern is sensitive to the initial density of motors. At high density, it is similar to coarsening of XY spins following a quench from high temperatures [21–25]. With periodic boundary conditions, the ultimate pattern is one of aligned tubules, with the motors going around in a uniform current. Such a pattern is not possible with closed boundary conditions,

which typically lead to a single vortex in the center. At lower densities, fluctuations play a strong role, and we observe a novel phenomenon of *arrested coarsening*, in which an inhomogeneous pattern of tubules freezes at some point in time. This occurs because the transport of motors produces regions in which the density of motors is very low (effectively zero). When such regions percolate throughout the system, no further rearrangement of tubules is possible.

To better understand the dynamics of coarsening and sizes of the arrested domains, we also simulated the equations in one dimension. Even in this case, the equations exhibit a variety of interesting patterns that depend on the boundary conditions: (i) With periodic boundary conditions, there is a phase transition between a state with a uniform current of motors running along tubules aligned in one direction (at high motor densities); and one in which there is a localized cluster of motors moving at constant velocity around the system (at low densities). Note that both patterns correspond to a broken symmetry (of the two possible tubule orientations) in one dimension. In contrast to the equilibrium Ising model, this symmetry breaking appears to persist in the presence of noise (mimicking finite temperatures). (ii) Reflecting boundary conditions lead to an oscillating front sweeping back and forth across the system; yet another solitonic solution to the equations. (iii) Closed boundary conditions give rise to initial coarsening, and eventual freezing of the tubules into domains. The domain size for frozen tubules depends on the value of the average motor density. Unlike its two dimensional counterpart, the motor density continues to evolve after the tubules are frozen, and all motors are eventually localized in one cluster.

II. MODEL

We introduce the local motor density $m(\vec{x}, t)$, and the tubule orientation field $\vec{T}(\vec{x}, t)$. The conservation of motors leads to the continuity equation

$$\frac{\partial m}{\partial t} = -\nabla \cdot \mathbf{J}_m, \quad (1)$$

where for the motor current, we shall assume the form

$$\mathbf{J}_m = -D \nabla m + A m \vec{T}. \quad (2)$$

Here, D is the diffusion constant for motors, while A is a coefficient describing their transport along the tubule direction \vec{T} . These are the lowest order terms in an expansion in m ; higher order terms are expected and may become important at high motor densities. While tubules generally grow and fragment [14]; their lengths can be stabilized by addition of taxol. We model this preference towards a particular length by an energy function, $-\alpha T^2/2 + \beta T^4/4$, similar to that used to describe spins

in the Landau-Ginzburg equation. In the same spirit, we associate an energy cost of $K(\nabla \vec{T})^2/2$ with variations in the orientation of tubules. Extremizing such an energy function leads to

$$\frac{\partial \vec{T}}{\partial t} = \alpha \vec{T} - \beta T^2 \vec{T} + \nabla \cdot (K \nabla \vec{T}). \quad (3)$$

Since the alignment of tubules is entirely by motors, we set $K = \gamma m$. Of course, since this is a non-equilibrium process, there is no *a priori* reason for the dynamics to originate from the minimization of an energy functional. A more systematic approach is to include all terms allowed by symmetries. In this case the equation for $\partial \vec{T}/\partial t$ may include terms $\gamma m \nabla^2 \vec{T}$ and $\gamma' \nabla m \cdot \nabla \vec{T}$ with different coefficients. For ease of description we shall start with the case $\gamma = \gamma'$, so that the dynamics is similar to minimizing an energy locally proportional to $\gamma m(\vec{x}, t)(\nabla \vec{T})^2/2$.

Finally, we can bring the equations into simpler form by rescaling to

$$\frac{\partial m}{\partial t} = \nabla^2 m - \nabla \cdot (m \vec{T}), \quad (4)$$

$$\frac{\partial \vec{T}}{\partial t} = C \vec{T} (1 - T^2) + \nabla \cdot (m \nabla \vec{T}), \quad (5)$$

where we now measure length in units of $\sqrt{\beta/\alpha} D/A$, time in units of $\beta D/(\alpha A^2)$, motor density in units of D/γ , and the tubule density vector in units of $\sqrt{\alpha/\beta}$. The remaining parameter C is given by $\beta D/A^2$.

III. SIMULATIONS

We perform numerical simulations on a two-dimensional $L \times L$ lattice, adapting the Crank–Nicholson scheme with the ADI operator splitting method [26]. The equations are discretized with spatial intervals of $\Delta x = \Delta y = 1$, and time intervals of $\Delta t = 10^{-2}$. At the edges of a finite system, we employ one of several possible boundary conditions: *Reflecting boundaries* have fixed inward pointing microtubules described by

$$\vec{T} \Big|_{\text{boundary}} = -\hat{n}, \quad (6)$$

where \hat{n} is the normal outward vector at the boundary. This discourages motors from approaching an edge. By contrast, with *parallel boundary conditions* the microtubules are tangential to the boundaries, while *closed boundary conditions* place no restriction on the tubules. In all these cases, there is no current transporting motors outside the system. There is no restriction on the motor current when *periodic boundary conditions* are applied, although again the total number of motors is conserved.

We start with an initial condition in which the motor density is uniformly set to m_0 at all points, while

the tubule field has magnitude $|\vec{T}_0| = 10^{-3}$ and random orientations. After a transient period, the homogeneous configuration self organizes into patterns that depend on the value of average motor density m_0 , as well as the growth constant C . Figure 1 shows a mixture of vortices and asters which arises as the stationary pattern for $m_0 = 0.01$. Both asters (tubules pointing inward) and vortices (tubules going around) are clearly visible and randomly arranged throughout the system. The motor density now becomes inhomogeneous, with motors accumulating in the centers of vortices and asters [Fig. 2]. The asters are more visible and dominant as the initial motor density increases, as shown for $m_0 = 0.15$ in Fig. 3. However, higher densities lead to a single vortex as in Fig. 4 for $m_0 = 0.5$ [27].

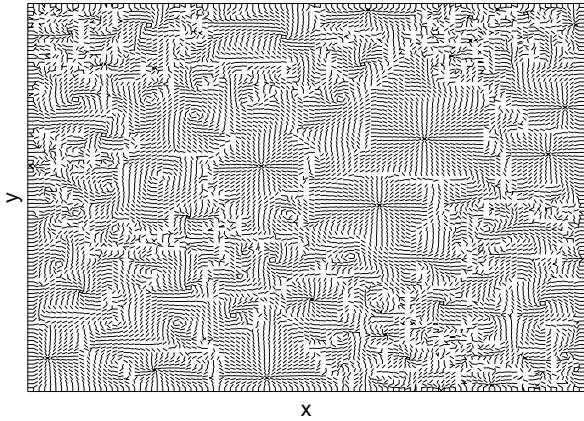


FIG. 1. A lattice of vortices and asters for $m_0=0.01$ and $C=100$. Initially, the size of the tubule is 10^{-3} , and their directions are random.

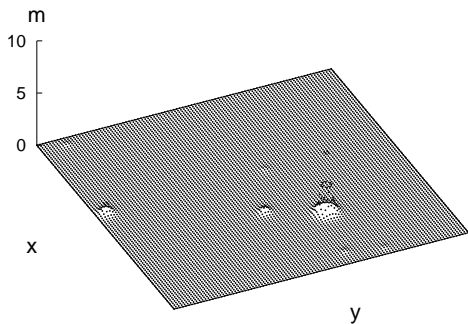


FIG. 2. The profile of motor density corresponding to Fig. 1. The initial homogeneous density evolves to obtain peaks at the centers of asters and vortices.

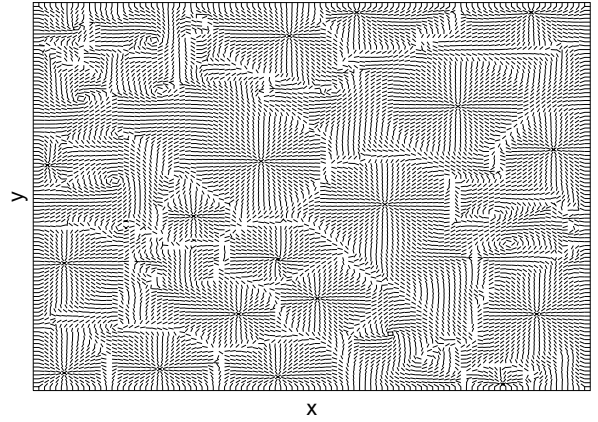


FIG. 3. A lattice of asters for $m_0 = 0.15$ and $C = 100$.

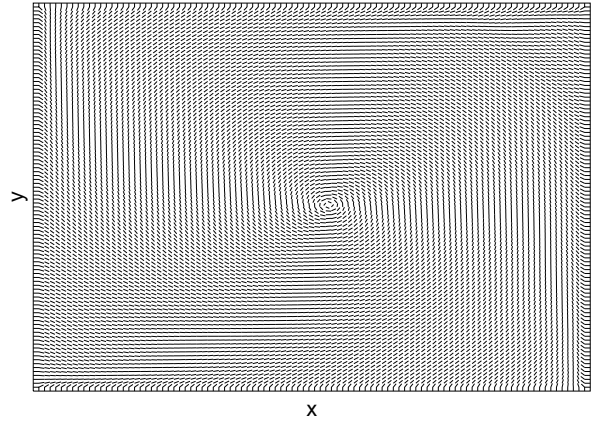


FIG. 4. A large vortex for $m_0 = 0.5$ and $C = 100$. At sufficiently high densities of motors, one or several vortices are formed.

The dynamics of formation of a large vortex from the random initial conditions is depicted in Fig. 5. This figure corresponds to reflecting boundary conditions, with $C=10$, and $m_0=0.15$. Since the initial tubule length is smaller than unity, the first stages of evolution are the lengthening of tubules as depicted in Figs. 5(a) and 5(b), for times $t = 0.6$ and $t = 1$, respectively. During this stage the directions of the tubules do not change and remain randomly distributed. The next stage involves reorientations of the tubules. Since a uniform alignment is incompatible with the boundary conditions, an aster forms in the center as depicted in Fig. 5(c), for $t = 120$. Motors are now transported along the tubules and accumulate at the center of the aster. At longer times, the aster pattern gives way to a vortex as in Fig. 5(d) for $t = 1200$. The vortex pattern is stable, although its center may move around depending on the choice of boundary conditions [27]. This dynamics is consistent with the experimental observation that vortices form from the destabilization of asters [16].

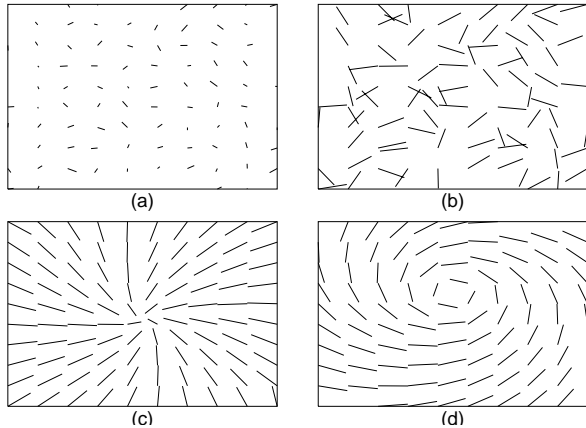


FIG. 5. The evolution of a vortex from an aster at times $t = 0.6$ (a), $t = 1$ (b), $t = 120$ (c), and $t = 1200$ (d). The random initial pattern of tubules first grows in length, and then organizes as an aster. Motors accumulate at the center of the aster, and then circle around when it changes to a vortex.

To model pattern formation in larger systems in which boundary effects are less important, we also performed simulations with closed boundary conditions. This change in the boundary condition does not qualitatively alter the pattern formation process. At low motor densities, we still observe a mixture of vortices and asters, followed by a collection of asters as m_0 is increased. However, at large motor density, after formation of a large vortex at the center, motors also pile up at several points on the boundary, as indicated in Fig. 6.

Equations (4) and (5) are deterministic; the only stochasticity appearing through the initial conditions. However, randomness and noise are certainly present in the experimental situations. In particular, microtubules are known to constantly grow and shrink through a dynamic instability [13,14], while asters are still observed under such conditions [28]. To make sure that the patterns observed in our simulations survive the addition of noise, we also introduced a stochastic noise in the tubule evolution equation. We observed that the self-organized patterns are stable at small noise, but that sufficiently large noise causes a phase transition to homogeneous mixtures (bundles of microtubules in a uniform motor density). Alternatively, we observe that for a fixed amount of noise, patterns are destroyed at motor densities lower than a critical m_c , but are qualitatively unchanged otherwise. (The value of m_c is 0.005 if the noise distributed uniformly between -1 and 1 .)

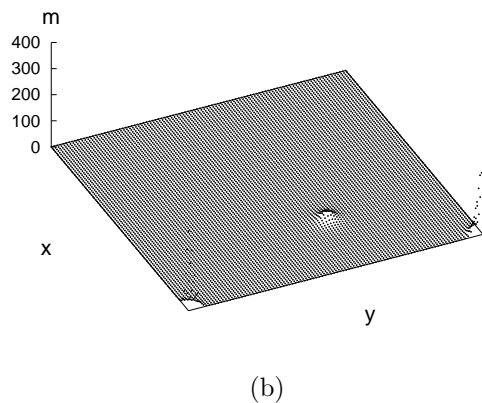
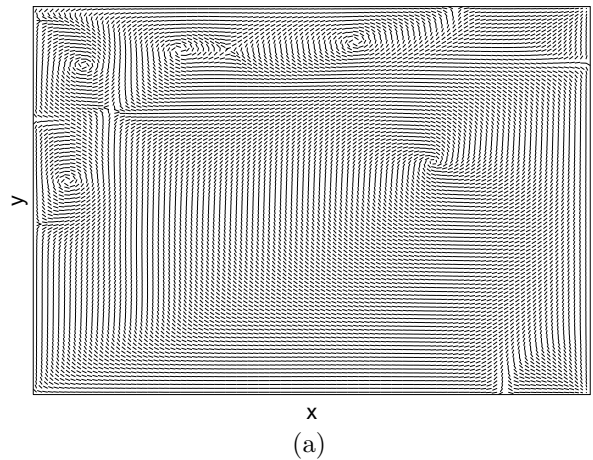


FIG. 6. The configuration of tubules for $m_0 = 0.5$, with closed boundary conditions (a); and the corresponding profile of motor density (b). Motors pile up at several points on the boundary, in addition to the interior.

IV. ASTER AND VORTEX SOLUTIONS

We can easily find analytical solutions to Eqs. (4) and (5) that describe the motor density in the center of an aster or vortex. To this end, we look for stationary solutions, $\partial_t m = \partial_t \vec{T} = 0$, with radial symmetry. In an aster the tubules are directed towards the center and $\vec{T} = -\hat{r}$, where \hat{r} is the unit radial vector. Balancing the diffusive current $-\partial_r m$, with that transported along tubules gives an exponential form

$$m_{\text{aster}}(r) = m(0) \exp(-r). \quad (7)$$

This exponential profile is indeed verified by the simulations as depicted in Fig. 7.

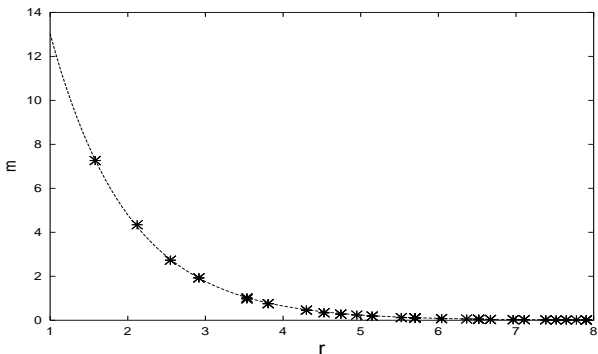


FIG. 7. The points represent the profile of motor density in an aster pattern for $m_0 = 0.1$ and $C = 100$. The dashed line is a least-square fit to the exponential decay $35.4 \exp(-r)$.

The tubules go around the center of a vortex, and $\vec{T} = \hat{\theta}$, where $\hat{\theta}$ indicates the tangential unit vector. Motors are then transported in a uniform circular current by the tubules. To ensure that there is no radial current of motors we need $\partial_r(r\partial_r m) = 0$, whose solution is

$$m_{\text{vortex}}(r) = -M \log(r/R), \quad (8)$$

where R is a long distance cut-off, of the order of the vortex size. A logarithmic fit to the simulated vortex motor density profile is shown in Fig. 8.

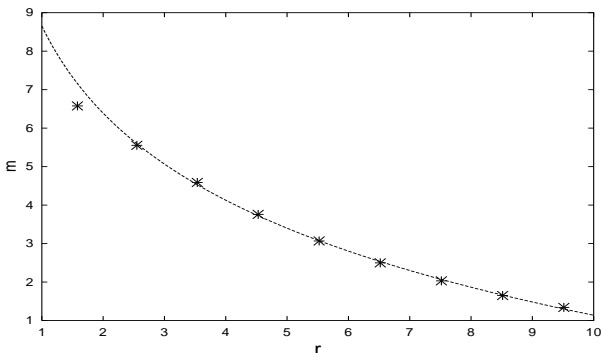


FIG. 8. The simulated profile of the motor density of a vortex for $m_0 = 0.2$ and $C = 1$. The dashed line is the least-square fit to the form, $-3.3 \log(r/14.2)$.

The profile of motors in quasi two dimensional asters has been studied theoretically and experimentally in Ref. [19]. In this study the tubules can grow to form quite long tracks, and their density also falls off away from the aster center. These differences in tubule behavior (as opposed to our case where tubules have uniform density and length) lead to predicted power law decays of the motor density profile.

The aster and vortex configurations of tubules are related to topological defects in the XY model. However, they are equivalent defects in the XY model as one can be deformed into the other through a 90° rotation. The presence and rearrangement of motors in our problem

breaks this symmetry and the two configurations become inequivalent. In particular, the two defects have very different static energies $E = \int d^2r m(r)(\nabla T)^2/2$. In the aster, the motors are concentrated close to the center leading to a high strain energy. By contrast, the motor density in a vortex is more uniform. Consequently, for the same number of motors, a large aster has much higher energy than a large vortex. Since the dynamics tends to minimize this energy, we have an explanation for why asters give way to the more stable vortices. Presumably, finite size effects in smaller asters, of the order of the decay length implicit in Eq. (7), account for their stability at small motor densities as in Fig. 3.

V. ARRESTED COARSENING

If the motor density is maintained at a uniform and fixed value, the dynamics of the tubules is identical to the coarsening of an XY system following a quench from high temperatures. This problem has been extensively studied [21–25] and (up to logarithmic corrections) the typical length scale of the pattern coarsens as $\xi \sim t^{1/2}$. In our case, the motors rearrange themselves in the landscape of the tubules and the coarsening scenario is modified when the motor density fluctuations become significant.

At high motor densities there are enough motors left over after formation of asters and vortices to cause further rearrangements of the tubules, and coarsening continues towards the final pattern consistent with the boundary conditions. However, at low densities the motors quickly migrate to the centers of asters and vortices. The little motor density left in the regions in between defects may then be too small to cause further realignment of tubules which became frozen. We call this phenomenon *arrested coarsening* of tubules. The limiting value of m_0 for the onset of arrested coarsening in fact depends on the growth constant of tubules C , as indicated by the “phase diagram” sketched in Fig. 9.

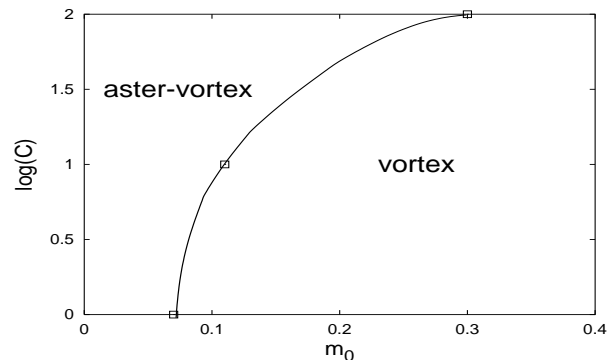


FIG. 9. The phase boundary in the plane of m_0 and $\log C$. To the right of the boundary the pattern coarsens to a large vortex. The arrested coarsening on the left side leads to frozen asters and vortices, with the aster pattern becoming more dominant as m_0 increases.

VI. ONE DIMENSION

To further understand the patterns, we examine the equations in one dimension, where more detailed simulations are possible. In particular, we consider scalar fields $m(x, t)$ and $T(x, t)$ evolving as

$$\partial_t m = \partial_x^2 m - \partial_x(Tm), \quad (9)$$

$$\partial_t T = C(T - T^3) + \partial_x(m\partial_x T). \quad (10)$$

Such equations may be appropriate to describe the movement of myosin motors along quasi-one dimensional bundles of actin filaments which occurs in muscle contraction, and may be responsible for other types of cell motion [8]. Bundles of actin molecules can be formed *in vitro* in mixtures with other inert polymers. These bundles consist of random mixtures of actin molecules oriented in the two possible direction. However, in the presence of myosin motors and ATP, there is a sorting of polarity [29,30] and active contraction of polar filaments [31]. While the bundles are usually linear with open ends, then sometimes assemble into a ring [29]. It may also be possible to artificially confine other mixtures of tubules and motors in quasi-one dimensional containers with various boundary conditions. In fact, we observe that the solutions to Eqs. (9) and (10) are quite sensitive to boundary conditions. Specifically, simulations show the following results:

(i) *Periodic boundary conditions* correspond to placing the system on a closed loop. We observe two types of symmetry breaking, depending on the initial density of motors. If m_0 is larger than a critical value of m_c ($m_c \approx 0.04$ for $C = 1$), the tubule pattern coarsens until the tubules are all aligned in one direction ($T = +1$ or -1). This is accompanied by a uniform current of motors that goes around the system. This symmetry breaking is similar to that of an Ising model. However, unlike the equilibrium Ising model, the broken symmetry survives in the presence of random noise (simulating finite temperatures) in Eq. (10). Any domains of opposite spin formed due to randomness are annealed by a rush of motors to the domain walls. The symmetry breaking in the presence of noise is due to advection term in Eq. (9), and active transportation of motors along the tubules. Indeed we checked that when the advection term is removed, the presence of noise in Eq. (10) leads to finite domains.

If m_0 is smaller than m_c , a novel final state emerges in which the motors gather together in a cluster that moves around the loop with a constant velocity. The tubules are again ordered in one direction, except near the cluster, where they briefly take the opposite alignment. Figure 10 shows that the configurations of the tubules and the profile of the motor density for $m_0 = 0.02 < m_c$. We have verified by direct numerical integration that Eqs. (9) and (10) do indeed support such a solitonic solution. However, the mathematical details are not in the spirit of this

article, and will be presented elsewhere.

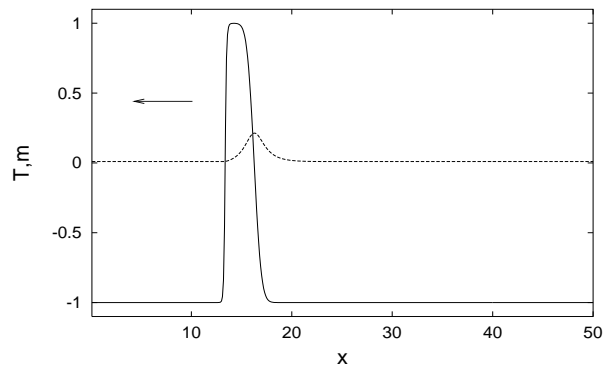


FIG. 10. The profiles of motor density (dashed line) and tubule orientation (solid line) in one dimension with *periodic boundary conditions*, for $m_0 = 0.02$ and $C = 1$. The whole pattern moves as indicated by the arrow, with a fixed speed.

(ii) *Reflecting boundary conditions* were imposed by requiring the tubules at the edges to point inward, i.e. [$T(0) = +1$ and $T(L) = -1$]. There is an initial coarsening period in which domains of $+1$ and -1 grow inward from the respective edges. However, in the final pattern the boundary between the $+1$ and -1 domains is not stationary, but sweeps back and forth across the system! The motors are again concentrated at the interface, with a solitonic profile as indicated in Fig. 11.

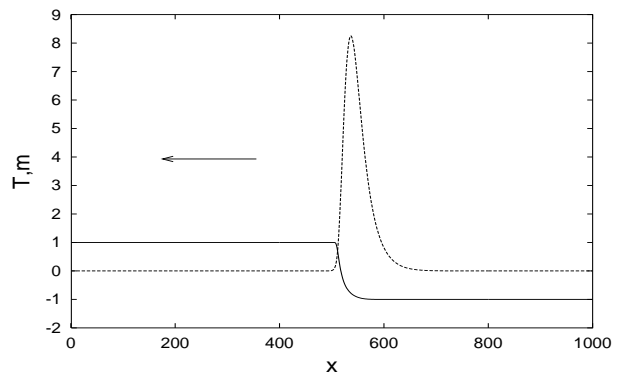


FIG. 11. The profiles of motor density (dashed line) and tubule orientation (solid line) in one dimension with *reflecting boundary conditions*, for $m_0 = 0.4$ and $C = 1$. The cluster of motors moves as indicated by the arrow, but its direction is reversed at each boundary, as the profile oscillates back and forth.

(iii) *Closed boundary conditions* were also applied, with no restrictions on the value of T at the edges, but setting the outward motor current to zero. Above a critical motor density, coarsening of tubules proceeds to a single domain of the size of the system, L . Following the tubules, the motors then pile up at one end of the system. The low density behavior in this case is similar to the arrested coarsening observed in the two dimensional case:

The initial growth of $+1$ and -1 domains is stopped at some point due to the local absence of motors necessary for continuing realignments. Figure 12 shows the average domain size, as a function of the average motor density. At the point when tubule evolution is stopped, the motor density has peaks at $(+, -)$ domain boundaries. However, as time goes on, there is a slower ripening process in which the motors gradually diffuse against the unfavorable domains, and eventually aggregate at one point in the system, as in Fig. 13. (It is not clear if this process is truly absent in two dimension, or merely takes too long to observe in simulations. There are similarities to the localization problem in which 2 is a critical dimension.)

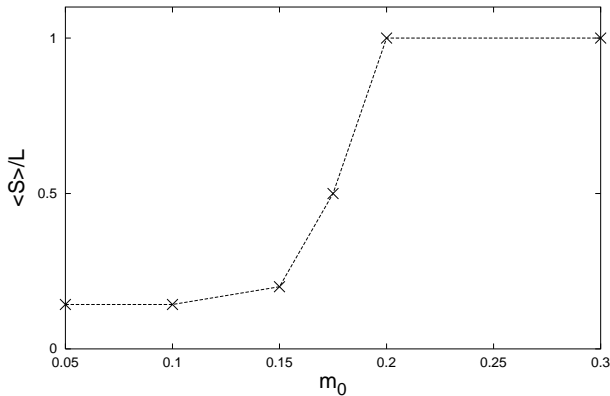


FIG. 12. The average tubule domain size in a one dimensional system of length L with closed boundary conditions, as a function of average motor density m_0 for $C = 1$.

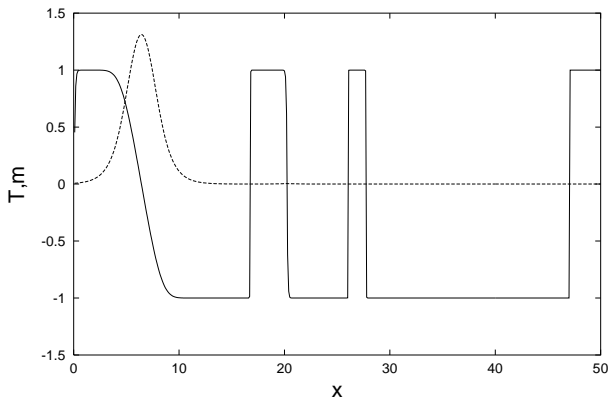


FIG. 13. The profiles of tubule orientation and motor density (solid and dashed lines, respectively) for $m_0 = 0.1$ and $C = 1$, in a one dimensional system with closed boundaries.

There are similarities in the above behaviors to patterns and phase transitions in other one dimensional non-equilibrium processes. A localization transition is observed in a population with diffusion, drift, and reproduction in Refs. [32–34]. This model of a bacterial colony

living on an oasis in the presence of randomly fluctuating wind, shows extended, localized, mixed states, as well as extinction, as a function of the average growth rate and convection velocity. In our model, the tubules (in their disordered state) provide a similar source of random advection. Ordered states are also observed in a lattice model with two species of particles in which the mobility of one species depends on the density of the other [35,36]. This model exhibits three phases: One with strong phase, a fluctuation-dominated phase, and another with uniform overall density. The couplings in our system between motors and tubules have similarities to the latter model, although the enforced conservation laws are different (there is no conservation of tubule orientations).

VII. DISCUSSION

Given how little input is used to construct the macroscopic equations (tubules transport motors and are aligned in the process), it is encouraging that many features of the experimental patterns are reproduced. As in the experiments, we observe arrays of asters and vortices, and large single vortices (formed from the break up of asters). However, at high densities of motors, the experiments lead to irregularly arranged bundles of tubules, a feature not present in our model. The absence of tubule bundles indicates the limitations of the macroscopic approach. To reproduce the observed sequence of patterns, more physical input into the equations is necessary. For example, a potential modification is to include non-linear terms in the transported motor current to model the inter-particle interactions at high densities.

In models of highway traffic [37], the current actually diminishes at high density, and can be approximated by

$$J[m] = -\nabla m + \vec{T} m e^{-m/m_{\max}}, \quad (11)$$

where m_{\max} is a characteristic density for saturation of current. Since the alignment of tubules is intimately connected to the motor current, similar modifications should appear in Eq. (5). As discussed earlier, because of the non-equilibrium nature of the process, the equation for $\partial_t \vec{T}$ does not have to be obtained from the minimization of an energy density. In fact, to describe saturation effects on alignment of tubules, we modified Eq. (5) to

$$\partial_t \vec{T} = C \vec{T} (1 - T^2) + \nabla m \cdot \nabla \vec{T} + m e^{-m/m_{\max}} \nabla^2 \vec{T} + \eta, \quad (12)$$

where η is a stochastic noise. The sequence of tubule patterns obtained from these modified equations upon increasing initial motor density is depicted in Fig. 14. We observe that the single vortex pattern becomes unstable at high densities, and we may regard the high density phase as representing bundles of tubules. We also find

that the patterns of vortices and asters are stable in the presence of noise in the following sense: If we average the whole configuration of tubules over time, the intermediate regions between defects are washed away while the defects survive.

The rich variety of behaviors observed in these simple equations are due to their nonequilibrium character. In the realm of equilibrium, for example, one dimensional systems at non-zero temperature are featureless and disordered. Clearly non-equilibrium effects can lead to symmetry breaking, and a rich interplay behaviors sensitive to boundaries. Biological systems can take advantage of such phenomena, and should indeed provide many interesting patterns in need of explanation.

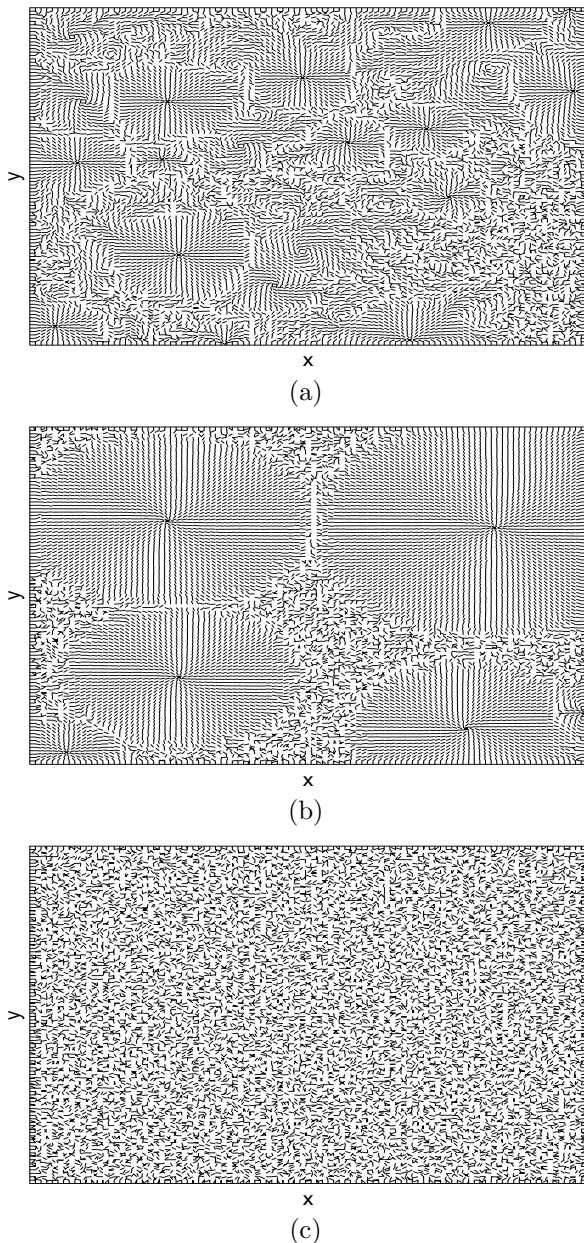


FIG. 14. The sequence of patterns obtained upon inclusion of saturation effects for $m_0 = 0.05$ (a), $m_0 = 1$ (b), and $m_0 = 20$ (c).

We wish to thank F. J. Nédélec and P. De Wulf for helpful discussions. H.Y.L. is supported by the Korea Science and Engineering Foundation through a fellowship. MK acknowledges the support of NSF grants DMR-98-05833 (at MIT) and PHY99-07949 (at ITP).

-
- [1] M. C. Cross and P. C. Hohenberg, *Rev. Mod. Phys.* **65**(3), 851 (1993).
 - [2] J. P. Gollub and J. S. Langer, *Rev. Mod. Phys.* **71**(2), S396 (1999).
 - [3] T. Vicsek, A. Czirok, E. Ben-Jacob, I. Cohen, and O. Shochet, *Phys. Rev. Lett.* **75**, 1226 (1995).
 - [4] J. Toner and Y. Tu, *Phys. Rev. Lett.* **75**, 4326 (1995).
 - [5] H. C. Berg, *Nature* **254**, 389 (1975).
 - [6] E. O. Budrene and H. C. Berg, *Nature* **349**, 630 (1991).
 - [7] E. Ben-Jacob, I. Cohen, O. Shochet, A. Tenenbaum, A. Czirok, and T. Vicsek, *Phys. Rev. Lett.* **75**, 2899 (1995).
 - [8] B. Alberts *et al.*, *The Molecular Biology of the Cell* (Garland, New York, 1994).
 - [9] A. Hyman and E. Karsenti, *Cell* **45**, 329 (1986).
 - [10] K. Svoboda, P. P. Mitra, S. M. Block, *Proc. Natl. Acad. Sci. USA* **91**, 11782 (1994).
 - [11] K. Visscher, M. J. Schnitzer, and S. M. Block, *Nature* **400**, 184 (1999).
 - [12] M. E. Fisher and A. B. Kolomeisky, *Physica A*, **274**, 241 (1999).
 - [13] T. Mitchison and M. W. Kirschner, *Nature* **312**, 237 (1984); **312**, 232 (1984).
 - [14] M. Dogterom and S. Leibler, *Phys. Rev. Lett.* **70**, 1347 (1993).
 - [15] R. Urrutia *et al.*, *Proc. Natl. Acad. Sci. USA* **88**, 6701 (1991).
 - [16] F. J. Nédélec, T. Surrey, A. C. Maggs, and S. Leibler, *Nature* **389**, 305 (1997).
 - [17] T. Surrey *et al.*, *Proc. Natl. Acad. Sci. USA* **95**, 4293 (1998).
 - [18] B. Bassetti, M. C. Lagomarsino, and P. Jona, *Eur. Phys. J B* **15**, 483 (2000).
 - [19] F. Nédélec, T. Surrey, and A. Maggs, e-print cond-mat/0010130.
 - [20] In Ref. [16], an artificial molecular construct consisting of four two-headed kinesin molecules linked by biotin-streptavidin was used. These molecules can simultaneously bind to two microtubules. However, it is not known if binding of microtubules by two-headed kinesin molecules occurs inside the cell, or if other mechanisms are responsible for their alignment.
 - [21] M. Mondello and N. Goldenfeld, *Phys. Rev. A* **42**, 5865 (1990).
 - [22] A. N. Pargellis, S. Green, and B. Yurke, *Phys. Rev. E* **49**, 4250 (1994).

- [23] A. J. Bray and A. D. Rutenberg, Phys. Rev. E **49**, R27 (1994).
- [24] A. D. Rutenberg and A. J. Bray, Phys. Rev. E **51**, R1641 (1995).
- [25] F. Rojas and A. D. Rutenberg, Phys. Rev. E **60**, 212 (1999).
- [26] W. H. Press, B. P. Flannery, S. A. Teukolsky, and W. T. Vetterling, *Numerical Recipes in C* (Cambridge University Press, Cambridge, 1988).
- [27] With boundary conditions of inward pointing tubules, the center of the single vortex moves around the center of the system. However, with tubules aligned parallel to the boundary, the pattern of the final vortex is stationary.
- [28] T. Mitchison and M. Kirshner, Nature **312**, 232 (1984).
- [29] K. Takiguchi, J. Biochem. **109**, 520 (1991).
- [30] H. Nakazawa and K. Sekimoto, **65**, 2404 (1996).
- [31] K. Kruse and F. Jülicher, **85**, 1778 (2000).
- [32] D. R. Nelson and N. M. Shnerb, Phys. Rev. E **58**, 1383 (1998).
- [33] K. A. Dahmen, D. R. Nelson, and N. M. Schnerb, J. Math. Biol. **41**, 1, (2000).
- [34] K. A. Dahmen, D. R. Nelson, and N. M. Schnerb, e-print cond-mat 9903276.
- [35] D. Das and M. Barma, Phys. Rev. Lett. **85**, 1602 (2000).
- [36] S. Ramaswamy, M. Barma, D. Das, and A. Basu, preprint.
- [37] B. S. Kerner and P. Konh user, Phys. Rev. E **48**, R2335 (1993).